Proton Shell Gaps in $N = 28$ Nuclei from the First Complete Spectroscopy Study with FRIB Decay Station Initiator

I. Cox,[1] Z. Y. Xu,[1] R. Grzywacz,[1,2] W.-J. Ong,[3] B. C. Rasco,[2] N. Kitamura,[1] D. Hoskins,[1] S. Neupane,[1,3] T. J. Ruland,[2,4] J. M. Allmond,[2] T. T. King,[2] R. S. Lubna,[5] K. P. Rykaczewski,[2] H. Schatz,[5,6] B. M. Sherrill,[5,6] O. B. Tarasov,[5] A. D. Ayangeakaa,[7,8] H. C. Berg,[5,6] D. L. Bleuel,[3] G. Cerizza,[5] J. Christie,[1] A. Chester,[5] J. Davis,[9] C. Dembski,[5,6] A. A. Doetsch,[5,6] J. G. Duarte,[3] A. Estrade,[10] A. Fijałkowska,[11] T. J. Gray,[2] E. C. Good,[5] K. Haak,[6] S. Hanai,[12] J. T. Harke,[3] C. Harris,[6] K. Hermansen,[5,6] D. E. M. Hoff,[3] R. Jain,[5,6] M. Karny,[11] K. Kolos,[3] A. Laminack,[2] S. N. Liddick,[5,13] B. Longfellow,[3] S. Lyons,[9] M. Madurga,[1] M. J. Mogannam,[13,5] A. Nowicki,[1] T. H. Ogunbeku,[3] G. Owens-Fryar,[5,6] M. M. Rajabali,[14] A. L. Richard,[3] E. K. Ronning,[13,5] G. E. Rose,[15] K. Siegl,[1] M. Singh,[1,16] A. Spyrou,[5,6] A. Sweet,[3] A. Tsantiri,[6,5] W. B. Walters,[17] and R. Yokoyama[12]

[1]*Department of Physics and Astronomy, University of Tennessee, Knoxville, Tennessee 37996, USA*
[2]*Physics Division, Oak Ridge National Laboratory, Oak Ridge, Tennessee 37831, USA*
[3]*Lawrence Livermore National Laboratory, Livermore, California 94550, USA*
[4]*Department of Physics and Astronomy, Louisiana State University, Baton Rouge, Louisiana 70803, USA*
[5]*Facility for Rare Isotope Beams, Michigan State University, East Lansing, Michigan 48824, USA*
[6]*Department of Physics and Astronomy, Michigan State University, East Lansing, Michigan 48824, USA*
[7]*Department of Physics and Astronomy, University of North Carolina at Chapel Hill, Chapel Hill, North Carolina 27599, USA*
[8]*Triangle Universities Nuclear Laboratory, Duke University, Durham, North Carolina 27708, USA*
[9]*Pacific Northwest National Laboratory, Richland, Washington 99354, USA*
[10]*Department of Physics, Central Michigan University, Mount Pleasant, Michigan 48859, USA*
[11]*Faculty of Physics, University of Warsaw, PL 02-093 Warsaw, Poland*
[12]*Center for Nuclear Study, University of Tokyo, Wako, Saitama 351-0198, Japan*
[13]*Department of Chemistry, Michigan State University, East Lansing, Michigan 48824, USA*
[14]*Physics Department, Tennessee Technological University, Cookeville, Tennessee 38505, USA*
[15]*University of California, Berkeley, Berkeley, California 94704, USA*
[16]*Los Alamos National Laboratory, Los Alamos, New Mexico 87545, USA*
[17]*Department of Chemistry and Biochemistry, University of Maryland, College Park, Maryland 20742, USA*

(Received 19 October 2023; revised 12 December 2023; accepted 8 March 2024; published 12 April 2024)

The first complete measurement of the β-decay strength distribution of $^{45}_{17}Cl_{28}$ was performed at the Facility for Rare Isotope Beams (FRIB) with the FRIB Decay Station Initiator during the second FRIB experiment. The measurement involved the detection of neutrons and γ rays in two focal planes of the FRIB Decay Station Initiator in a single experiment for the first time. This enabled an analytical consistency in extracting the β-decay strength distribution over the large range of excitation energies, including neutron unbound states. We observe a rapid increase in the β-decay strength distribution above the neutron separation energy in $^{45}_{18}Ar_{27}$. This was interpreted to be caused by the transitioning of neutrons into protons excited across the $Z = 20$ shell gap. The SDPF-MU interaction with reduced shell gap best reproduced the data. The measurement demonstrates a new approach that is sensitive to the proton shell gap in neutron rich nuclei according to SDPF-MU calculations.

DOI: 10.1103/PhysRevLett.132.152503

Introduction.—The emergence of shell closures in nuclei caused by the spin-orbit force, as postulated by Mayer and independently by Haxel, Jensen, and Suess has played a foundational role in nuclear physics for decades [1,2]. With advances in radioactive ion beam facilities, it became clear that magic numbers, originally established at 2, 8, 20, 28, and so on for stable and near stable nuclei, change for very neutron-rich nuclei. One well-known example is the first island of inversion, where the $N = 20$ shell gap vanishes around ^{32}Mg [3–5]. Since then, there have been major efforts to establish the evolution of neutron shell gaps near $N = 20$ [6–11]. Later, the disappearance of magicity along the $N = 28$ isotonic chain below ^{48}Ca was revealed [12,13]; thus, the second island of inversion was established [14]. Modern nuclear models require as complete a set of configurations as possible. This was exemplified in the success of recent *ab initio* calculations [15,16] or the empirical large-scale shell model (LSSM), which includes multiple oscillator shells to reproduce the deformation in the islands of inversion [17–20]. While neutron shell

evolution around $N = 28$ has been a prominent area of study through Coulomb excitation [21–23], decay spectroscopy [24–27], particle transfer reactions [13,28–30], and nuclear moment measurements [31–33], proton shell evolution is less scrutable. Although, there is clear experimental evidence for new proton shell closures at $Z = 6$ [34] and $Z = 14$ [35], and ^{48}Ca ($Z = 20$) is a well-established doubly magic nucleus, little is known away from the magic numbers. A crucial question arises on how neutron excess changes the proton shell structure. Specifically, what observables are sensitive to the size of the proton shell gaps in the $N = 28$ nuclei and to how they evolve? This work studies the influence of proton (π) $f_{7/2}$ orbitals on excited states in ^{45}Ar, populated in the decay of ^{45}Cl$_{28}$, which lies in the transitional region [28] between the spherical ^{48}Ca and the deformed second island of inversion. We show that the β decays of these nuclei depend on the position of the proton $f_{7/2}$ and $p_{3/2}$ orbitals relative to the $d_{3/2}$ along with the already established disappearance of the $N = 28$ shell gap.

Conventionally, in nuclei with $N \geq 28$ and $Z < 20$, the Fermi surfaces for neutrons and protons are located within the pf and sd orbitals, respectively. For ^{45}Cl, allowed Gamow-Teller (GT) transition transforms sd and pf neutrons into protons in respective spin-orbit partner orbitals, generating highly excited, possibly neutron-unbound, states in the child nucleus. β-decay selection rules create a unique opportunity to study proton excitations across the $Z = 20$ as the $N = 28$ shell gap erodes. Proton shell gap information is not easily obtained with other experimental methods, which have identified states in ^{45}Ar using nuclear reaction or decay spectroscopy [26–29,36–40]. In the first measurement of its kind, this work reconstructs the β-decay strength distribution for a wide energy range (0–8 MeV) by combining data from the Modular Total Absorption Spectrometer (MTAS) [41,42] with high-resolution neutron and γ-ray spectrometers that are part of the Facility for Rare Isotope Beams (FRIB) Decay Station Initiator (FDSi) [43,44]. Our results will be compared to LSSM calculations to benchmark theoretical calculations along the $N = 28$ shell closure. Accurately calculating the entire β-decay strength leads to the most precise half-life and neutron branching ratio predictions in the area.

Experiment.—The experiment was performed at FRIB using an ^{82}Se primary beam, at 165 MeV/nucleon, impinged on a 3.811 mm thick ^{9}Be target. The resulting cocktail of nuclei was sent through the Advanced Rare Isotope Separator [45] to select the fragments of interest. Beam ions were identified based on their energy loss in silicon detectors and the time of flight between two upstream timing scintillators, one in the Advanced Rare Isotope Separator and another in the first diagnostic cross, shown in Fig. 1. Figure 2(a) shows the particle identification spectrum for isotopes of interest. The resulting beam was implanted at the two FDSi ion-implantation detection systems [43], as shown in Fig. 1, each located in approximate focal points of the separator bending magnet system. The first focal plane used the same detector setup described in Refs. [44,46] for neutron and γ-ray spectroscopy. Transport of the beam to the second focal plane was achieved by removing the first implantation detector and adjusting ion optics, thus allowing for total absorption measurements. The beam was implanted for 18 (15) h, yielding 190 000 (16 000) ions for the first (second) focal plane. Transmission of ^{45}Cl to the second focal plane was significantly lower due to the combination of a longer flight path from the last focusing magnet to the implantation point and because ^{45}Cl was a fringe nucleus, being produced on the edge of the chosen separator acceptance.

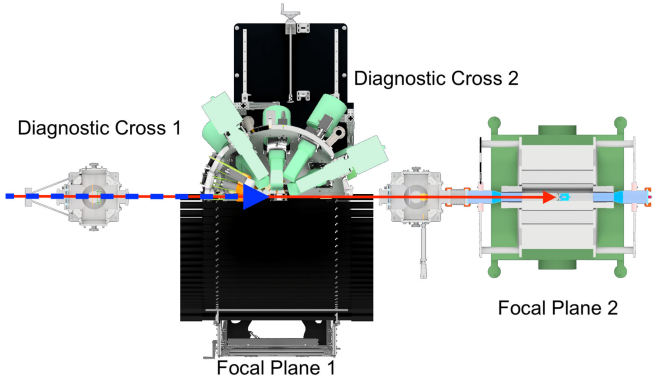

FIG. 1. Top view of the FDSi two-focal plane system, sliced to see the implantation locations. The beam comes from the left, passing through the first diagnostic cross, and can follow the blue (red) path to implant into the first (second) focal plane. In the first focal plane, south of the beam path is the neutron detector array, while north of the beam is the γ-ray detection system. The second focal plane consists of an implantation detector inserted into MTAS, preceded by an accompanying diagnostic cross.

The DEcay Germanium Array initiator (DEGAi) measured individual γ-rays with an overall detection efficiency of 3.6% at 1 MeV for the clover array consisting of 11 HPGe clover detectors. Neutron energies were measured with a double wall of 88 Versatile Array of Neutron Detectors at Low Energy (VANDLE) time-of-flight scintillator detectors [48,49], with a total neutron detection efficiency of 19% at 1 MeV. GEANT4 simulations [50] were parametrized with the spectrum from ^{49}K [51] to provide an efficiency curve and a response function [52] for the neutron detectors. With a new segmented central module [53], MTAS consists of 24 individual NaI detectors, with an overall efficiency of 94% for partial γ absorption at 500 keV. A new implantation detector was developed to fit inside the central module of MTAS, with the design inspired by the detectors used in [44,54], using a segmented yttrium orthosilicate (Y_2SiO_5, or simply YSO) inorganic scintillator coupled to an 8×8 array of silicon photomultipliers [55]. Data from both focal planes were recorded using XIA Pixie16 digitizers [56].

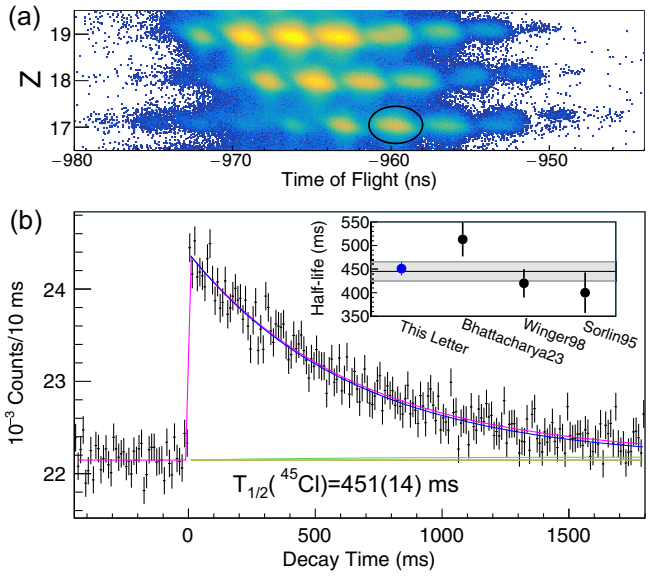

FIG. 2. Panel (a) shows the particle identification corresponding to implanted nuclei from chlorine to potassium. The atomic number (Z) was determined from the energy loss in the pin detector, with the time of flight between upstream timing scintillators. The black circle represents the location for ^{45}Cl. Panel (b) shows the decay curve for ^{45}Cl from the first focal plane. The blue line shows the decay of the main isotope, and the green (yellow) line shows the inclusion of the P_{0n} (P_{1n}) child decays. The total fit, including a constant background, P_{0n}, and P_{1n} decays, is shown by the pink line. The inset plot compares experimental values for the half-life of ^{45}Cl, including literature from Refs. [27,38,47], with the weighted average shown as the black line with a gray band.

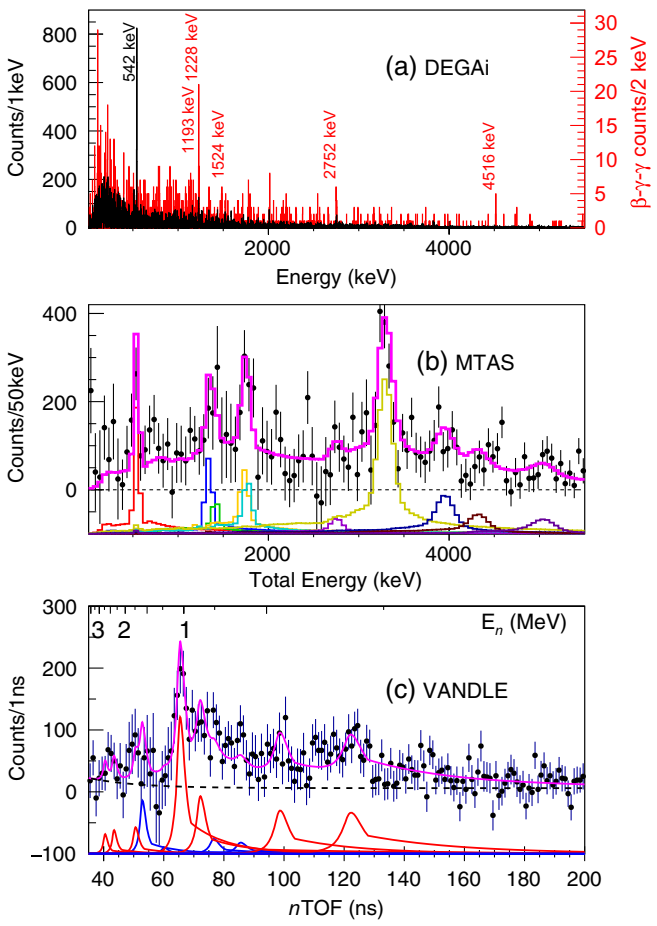

FIG. 3. Decay signatures within 1800 ms of ^{45}Cl implantation obtained using all three parts of the FDSi. (a) shows the high-resolution γ-ray data, with the singles shown in black and the γ-γ spectrum gated on the 542 keV transition shown in red. The most prominent peaks assigned to ^{45}Ar have been marked with the corresponding γ-ray energy. (b) shows the MTAS data and deconvolution, where the different color lines represent feeding to individual states and the pink line is the total fit as the sum of the paths. States above S_n were not considered due to low statistics. (c) shows the results of the neutron deconvolution, measuring neutron energies (E_n) via the time-of-flight (nTOF) method. The red (blue) peaks are neutrons that feed to the ground (excited) state(s) in ^{44}Ar. The deconvolution data for (b) and (c) has been shifted down on the y axis for visualization purposes, but the total fit (pink) has not been shifted.

Results.—Both the ion implantation and β-decay events are measured in a position-sensitive YSO detector, allowing for β-ion correlations in time and space [44]. From this, the half-life ($T_{1/2}$) can be determined for ^{45}Cl, as shown in Fig. 2(b). The experimental uncertainty in the half-life was determined by an uncorrelated combination of statistical error in the fit, along with systematic errors due to the assumptions of the branching ratio [38], P_{0n} child, ^{45}Ar, half-life [57], and P_{1n} child, ^{44}Ar, half-life [58]. The half-life fit used a branching ratio of $P_n = 28(9)\%$. A comparison with previous results from Sorlin *et al.* [38], Winger *et al.* [40], and Bhattacharya *et al.* [27] is shown in the inset plot in Fig. 2(b). The weighted average from the previous literature values, shown as the black line with a gray band in the inset of Fig. 2(b), agrees well with this work, $T_{1/2} = 451(14)$ ms.

Individual γ-ray transitions corresponding to the decay of ^{45}Cl, shown in Fig. 3(a), are consistent with previously reported values [26,27,39,40]. The most intense γ-ray transition is between the ground and first excited states at 542 keV. The red data in Fig. 3(a) shows the γ-ray energy spectrum in coincidence with the 542 keV transition, with a new line at 4516(3) keV that represents the de-excitation from a new state at 5058(3) keV.

Using the high efficiency of MTAS, the complete feeding pattern to states in ^{45}Ar below the neutron-separation energy, $S_n = 5168.9(17)$ keV [59], is measured. The sum-energy spectrum from MTAS, Fig. 3(b), reflects the direct level population in ^{45}Ar. It was deconvoluted using the Bayesian algorithm detailed by Shuai *et al.* [60]. The strong feeding at 3.3 MeV agrees well with previous measurements [26,27]. This result also supports the new state at 5 MeV, with significant β feeding.

Neutron energies were measured via the neutron time-of-flight (nTOF) method. Some of the neutrons in this experiment were detected in coincidence with γ rays, allowing for a deconvolution of the total neutron spectrum constrained by fitting γ-gated nTOF spectra; the technique is described by Xu *et al.* [52,61]. Figure 3(c) displays the result of the deconvolution, where the red (blue) peaks correspond to neutrons feeding the ground (excited) state(s) of ^{44}Ar. β feeding intensities (I_β) to seven quasiresonances [62] above S_n were found. The experimentally obtained neutron branching ratio, $P_n = 28(9)\%$, is in agreement with 24(4)% reported by Sorlin *et al.* [38].

From the β-feeding intensities measured by MTAS below and VANDLE above S_n, the experimental partial half-lives, $t = T_{1/2}/I_\beta$, can be determined. These are directly related to the β-decay strength, $S_\beta = 1/ft$ [63], of each state, where f is the Fermi function [64] for the electron distribution, based on $Q_\beta = 11.51(14)$ MeV [59]. Figure 4(a) shows the full cumulative S_β, up to 8 MeV, compared with several theoretical calculations. The systematics of the magnitude of the matrix elements and comparison with theory can guide the assignment of transitions as GT or first forbidden (FF). The S_β below 2 MeV reflects known negative and positive parity states attributed to FF and weak GT transitions. The first significant GT transition appears at 3.3 MeV due to the strong feeding to the $5/2^+$ state [27]. The next rapid change in S_β appears for neutron-unbound states and continues up to the sensitivity limit for the system, determined by the statistics and the decreasing phase space. These excitations are assumed to be a result of GT transitions due to their larger strength compared to the low-energy FF transitions. The spins and parities of the resulting states should be $J^\pi = 1/2^+$, $3/2^+$, or $5/2^+$.

Discussion.—For extremely neutron-rich nuclei, such as ^{45}Cl, including multiple major proton shells in nuclear models is essential to describe the general features of the observed decay strength distribution. Yoshida *et al.* have calculated the β-decay properties of ^{45}Cl using LSSM with the SD-PF-SDG interaction [20], assuming a $1/2^+$ ground state. The results, shown as the red curve in Fig. 4(a), provide a good overall description of the main features of S_β but disagree at lower excitation energies where they predict intense feeding to the $1/2^+$ state near 1.7 MeV, which is unobserved. To account for the newly established $3/2^+$ ground state for ^{45}Cl [27] and to explore the underlying nuclear structure, new LSSM calculations were performed using the SDPF-MU interaction [19]. The computational complexity allows only single particle--hole excitations across ^{40}Ca; however, no restrictions were imposed on the excitation across $N, Z = 28$. This enabled full collectivity in the pf orbitals and has been used for calculations of β-decay properties in this region [20]. For completeness, FF transitions were included in the

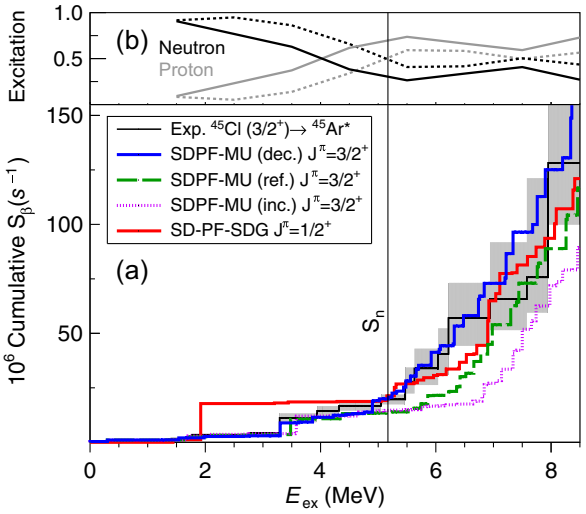

FIG. 4. (a) A comparison of experimental S_β (black) to theoretical predictions from LSSM using the SD-PF-SDG [20] (red) and SDPF-MU (blue, green, pink) interactions. In this figure, SDPF-MU (dec.) represents calculations done with the $Z = 20$ shell gap decreased by 1 MeV (blue) and SDPF-MU (inc.) $Z = 20$ shell gap increased by 1 MeV (pink dotted), compared to the reference gap shown by SDPF-MU (ref.) (green dashed curve). (b) The number of protons (gray) and neutrons (black) excited from the sd to pf shell, as a function of energy, for states in ^{45}Ar after β decay. The solid and dashed were obtained with decreased shell gap and reference SDPF-MU interactions, respectively. See text for more details.

calculations; their contributions are important only in populating low-excitation energies in ^{45}Ar. The effective scaling factors of GT and FF operators are taken from Ref. [20]. The calculation, shown as the green dashed line in Fig. 4(a), reproduces the low lying states in ^{45}Ar, emphasized by the agreement at low energies. Above the neutron separation energy, it reflects the general trend but with less cumulative strength.

In the SDPF-MU interaction, the nominal energy gap between sd and pf shells is 3.416 MeV in ^{16}O [19], resulting in an 8.519 MeV difference in the effective single-particle energies of $\pi f_{7/2}$ and $\pi d_{3/2}$ in ^{45}Cl [17]. Additional calculations were performed with ± 1 MeV modifications on the input single-particle energies of πpf orbitals, i.e., changing the relative spacing between sd and pf shells ($Z = 20$ shell gap). They are shown in Fig. 4(a) as the solid blue and dotted pink curves for the reduced and increased shell gap calculations, respectively. The low-energy S_β is insensitive to the modifications, indicating that they are uninfluenced by the πpf orbitals. Yet, the new experimental data at higher energies requires a 1 MeV compression of the shell gap. We also checked the sensitivity of other observables at low-excitation energy to the modified proton shell gap. Those observables include neutron spectroscopic factors [28,29], g factors [32,65,66], and nuclear masses [59] in terms of Q_β and S_n. While the

nominal SDPF-MU interaction well reproduces the available experimental data, reducing the proton shell gap by 1 MeV only induces minor variance in the calculated results. On the other hand, varying the $N = 28$ shell gap by 1 MeV (either increase or decrease) significantly deteriorates the agreement of those quantities, including the low-energy S_β at $E_x < 5$ MeV. These results suggest reducing the proton $Z = 20$ shell gap is a viable approach to resolve the discrepancy of S_β above S_n without affecting the calculated results that agree with the experimental data at low energy.

To understand why the decay distribution at high energies is sensitive to πpf orbitals in ^{45}Ar, new variables were constructed by counting the number of protons (neutrons) excited across $Z(N) = 20$, weighted by S_β as a function of excitation energy. This new variable, shown in Fig. 4(b), represents the excitation mode in child relevant to β decay and demonstrates that neutron cross-shell excitation dominates states populated below 4 MeV. This is consistent with previous results from the neutron transfer reaction on ^{46}Ar [29]. In contrast, the proton excitation into the pf shell increases near S_n and prevails at higher excitation energy. Reducing the $Z = 20$ shell gap mostly impacts the high-energy decay strength, as proton excitations from the sd to pf orbitals require less energy; this allows the GT strength to shift downward in line with the experimental data.

Investigations were made to find how changing the shell gap impacts predictions of the decay properties for other $N = 28$ isotones transitioning into the island of inversion, where the consequence of deformation is an increased mixing of the wave functions with orbitals belonging to different major shells. The same LSSM calculations were carried out for ^{47}K and ^{43}P. Figure 5 shows the strength distributions with and without the proton-shell modification. The shaded regions highlight the sensitivity of the cumulative S_β distributions for ^{47}K and ^{43}P to changes in the effective single-particle energies of the pf orbitals, similar to ^{45}Cl. The recent measurement by Smith *et al.* provides a lower limit for the strength distribution of ^{47}K [67], which agrees with the reference calculation but is not incompatible with the reduced calculations. The sensitivity in S_β for the odd $N = 28$ isotones emphasizes the value for complete decay-spectroscopy measurements for nuclei in the region to rigorously assess theoretical calculations. This is exemplified in the decay of ^{43}P, which has a large Q_β, yielding a wide distribution to benchmark the theory.

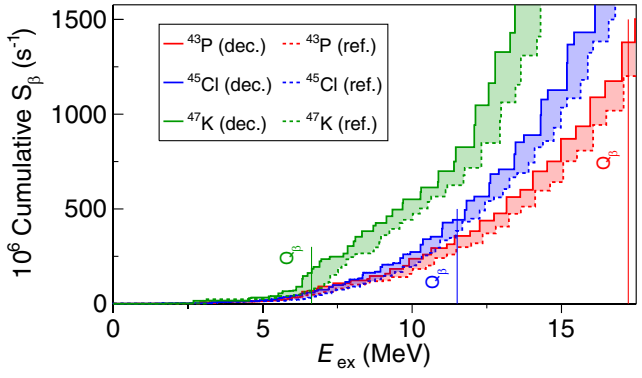

FIG. 5. The cumulative S_β for odd-Z decays along $N = 28$, calculated using the SDPF-MU interaction. Solid and dashed lines refer to the decreased (dec.) and reference (ref.) shell gaps, respectively. Vertical lines indicate Q_β values [59].

Conclusion.—Presented results demonstrate how complete measurements of β decays can provide discerning observables to guide nuclear models. At the two focal planes of FDSi, the first complete decay spectroscopy was performed on ^{45}Cl, integrating total absorption spectroscopy with high-resolution neutron and γ-ray spectroscopy. The cumulative decay strength, consistently measured both above and below S_n, could be compared to comprehensive predictions of theoretical models. We find that a 1 MeV reduction in the $Z = 20$ shell gap, when using the SDPF-MU interaction, is sufficient to reproduce the newly measured S_β distribution without affecting other low-energy observables. Though this agreement is compelling, other factors, such as correlations not captured by the Hamiltonian, may contribute to adjusting the β-decay strength for ^{45}Cl. The separation between the proton sd and pf orbitals is difficult to obtain in any other experimental method in this region. Future systematic measurements of the decay strength in the $N = 28$ region will open opportunities to guide updates for theoretical calculations for very neutron-rich nuclei.

We would like to thank the entire operations team at FRIB for reliable beam delivery during the experiment, and for all the work leading up to the experiment. Calculations for this work were performed using the KSHELL code [68]. This material is based upon work supported in part by the U.S. Department of Energy, Office of Science, Office of Nuclear Physics under Contracts No. DE-AC52-07NA27344 (LLNL), No. DE-AC05-00OR22725 (ORNL), No. DE-FG02-96ER40983 (UTK), No. DE-SC0016988 (TTU), No. DE-SC0020451 (MSU), Award No. DE-SC0020451 (FRIB), and used resources of the Facility for Rare Isotope Beams (FRIB) Operations, which is a DOE Office of Science User Facility under Award No. DE-SC0023633. This work was also sponsored by the Stewardship Science Academic Alliances program through DOE Awards No. DE-NA0003899 (UTK) and No. DOE-DE-NA0003906 (MSU), NSF Major Research Instrumentation Program Grant No. 1919735 (UTK), and the US National Science Foundation under Grants No. PHY-1714153 (CMU), No. PHY-20-12040 (B. M. S., O. B. T.), and No. PHY-2209429 (H. S.). This material is based upon work supported by the Department of Energy National Nuclear Security Administration through the

Nuclear Science and Security Consortium under Grant No. DE-NA0003996 and U.S. Department of Energy, National Nuclear Security Administration under Award No. DE-NA0003180 (MSU). S. L. and J. D. were supported by the Laboratory Directed Research and Development Program at Pacific Northwest National Laboratory operated by Battelle for the U.S. Department of Energy.

[1] M. G. Mayer, Phys. Rev. **75**, 1969 (1949).
[2] O. Haxel, J. H. D. Jensen, and H. E. Suess, Phys. Rev. **75**, 1766 (1949).
[3] C. Thibault, R. Klapisch, C. Rigaud, A. M. Poskanzer, R. Prieels, L. Lessard, and W. Reisdorf, Phys. Rev. C **12**, 644 (1975).
[4] C. Détraz, D. Guillemaud, G. Huber, R. Klapisch, M. Langevin, F. Naulin, C. Thibault, L. C. Carraz, and F. Touchard, Phys. Rev. C **19**, 164 (1979).
[5] C. Détraz, M. Langevin, D. Guillemaud, M. Epherre, G. Audi, C. Thibault, and F. Touchard, Nucl. Phys. **A394**, 378 (1983).
[6] A. Watt, R. P. Singhal, M. H. Storm, and R. R. Whitehead, J. Phys. G **7**, L145 (1981).
[7] A. Poves and J. Retamosa, Phys. Lett. B **184**, 311 (1987).
[8] E. K. Warburton, J. A. Becker, and B. A. Brown, Phys. Rev. C **41**, 1147 (1990).
[9] B. V. Pritychenko, T. Glasmacher, B. A. Brown, P. D. Cottle, R. W. Ibbotson, K. W. Kemper, L. A. Riley, and H. Scheit, Phys. Rev. C **63**, 011305(R) (2000).
[10] M. Belleguic *et al.*, Phys. Rev. C **72**, 054316 (2005).
[11] A. Chaudhuri, C. Andreoiu, T. Brunner, U. Chowdhury, S. Ettenauer, A. T. Gallant, G. Gwinner, A. A. Kwiatkowski, A. Lennarz, D. Lunney, T. D. Macdonald, B. E. Schultz, M. C. Simon, V. V. Simon, and J. Dilling, Phys. Rev. C **88**, 054317 (2013).
[12] F. Sarazin *et al.*, Phys. Rev. Lett. **84**, 5062 (2000).
[13] L. Gaudefroy *et al.*, Phys. Rev. Lett. **97**, 092501 (2006).
[14] B. Bastin *et al.*, Phys. Rev. Lett. **99**, 022503 (2007).
[15] T. Miyagi, S. R. Stroberg, J. D. Holt, and N. Shimizu, Phys. Rev. C **102**, 034320 (2020).
[16] A. Ekström, C. Forssén, G. Hagen, G. R. Jansen, T. Papenbrock, and Z. H. Sun, arXiv:2305.06955.
[17] T. Otsuka, T. Suzuki, R. Fujimoto, H. Grawe, and Y. Akaishi, Phys. Rev. Lett. **95**, 232502 (2005).
[18] E. Caurier, F. Nowacki, and A. Poves, Phys. Rev. C **90**, 014302 (2014).
[19] Y. Utsuno, T. Otsuka, B. A. Brown, M. Honma, T. Mizusaki, and N. Shimizu, Phys. Rev. C **86**, 051301(R) (2012).
[20] S. Yoshida, Y. Utsuno, N. Shimizu, and T. Otsuka, Phys. Rev. C **97**, 054321 (2018).
[21] B. Longfellow, D. Weisshaar, A. Gade, B. A. Brown, D. Bazin, K. W. Brown, B. Elman, J. Pereira, D. Rhodes, and M. Spieker, Phys. Rev. C **103**, 054309 (2021).
[22] S. Calinescu *et al.*, Phys. Rev. C **93**, 044333 (2016).
[23] D. Mengoni *et al.*, Phys. Rev. C **82**, 024308 (2010).
[24] L. Weissman, O. Arnd, U. Bergmann, A. Brown, R. Catherall, J. Cederkall, I. Dillmann, O. Hallmann, L. Fraile, S. Franchoo, L. Gaudefroy, U. Köster, K.-L. Kratz, B. Pfeiffer, and O. Sorlin, Phys. Rev. C **70**, 024304 (2004).
[25] V. Tripathi *et al.*, Phys. Rev. C **106**, 064314 (2022).
[26] J. Mrázek *et al.*, Nucl. Phys. **A734**, E65 (2004), Proceedings of the Eighth International Conference on Nucleus-Nucleus Collisions (NN2003).
[27] S. Bhattacharya *et al.*, Phys. Rev. C **108**, 024312 (2023).
[28] L. Gaudefroy *et al.*, Phys. Rev. C **78**, 034307 (2008).
[29] F. Lu, J. Lee, M. B. Tsang, D. Bazin, D. Coupland, V. Henzl, D. Henzlova, M. Kilburn, W. G. Lynch, A. M. Rogers, A. Sanetullaev, Z. Y. Sun, M. Youngs, R. J. Charity, L. G. Sobotka, M. Famiano, S. Hudan, M. Horoi, and Y. L. Ye, Phys. Rev. C **88**, 017604 (2013).
[30] K. Nowak *et al.*, Phys. Rev. C **93**, 044335 (2016).
[31] L. Gaudefroy *et al.*, Phys. Rev. Lett. **102**, 092501 (2009).
[32] M. De Rydt, J. M. Daugas, F. de Oliveira Santos, L. Gaudefroy, S. Grévy, D. Kameda, V. Kumar, R. Lozeva, T. J. Mertzimekis, P. Morel, T. Nagatomo, G. Neyens, L. Perrot, O. Sorlin, C. Stödel, J. C. Thomas, N. Vermeulen, and P. Vingerhoets, Phys. Rev. C **81**, 034308 (2010).
[33] R. Neugart, J. Billowes, M. L. Bissell, K. Blaum, B. Cheal, K. T. Flanagan, G. Neyens, W. Nörtershäuser, and D. T. Yordanov, J. Phys. G **44**, 064002 (2017).
[34] D. T. Tran *et al.*, Nat. Commun. **9**, 1594 (2018).
[35] P. Baumann, A. Huck, G. Klotz, A. Knipper, G. Walter, G. Marguier, H. Ravn, C. Richard-Serre, A. Poves, and J. Retamosa, Phys. Lett. B **228**, 458 (1989).
[36] Z. Dombrádi *et al.*, Nucl. Phys. **A727**, 195 (2003).
[37] A. Gade *et al.*, Phys. Rev. C **71**, 051301(R) (2005).
[38] O. Sorlin *et al.*, Nucl. Phys. **A583**, 763 (1995).
[39] S. Grévy *et al.*, Phys. Lett. B **594**, 252 (2004).
[40] J. A. Winger, H. H. Yousif, W. C. Ma, V. Ravikumar, W. Lui, S. K. Phillips, R. B. Piercey, P. F. Mantica, B. Pritychenko, R. M. Ronningen, and M. Steiner, AIP Conf. Proc. **455**, 606 (1998).
[41] M. Karny, K. Rykaczewski, A. Fijałkowska, B. Rasco, M. Wolińska-Cichocka, R. Grzywacz, K. Goetz, D. Miller, and E. Zganjar, Nucl. Instrum. Methods Phys. Res., Sect. A **836**, 83 (2016).
[42] B. C. Rasco *et al.*, Phys. Rev. C **95**, 054328 (2017).
[43] FRIB, Frib decay station initiator, https://fds.ornl.gov/initiator/ (2022) (accessed on 10-6-2023).
[44] H. L. Crawford *et al.*, Phys. Rev. Lett. **129**, 212501 (2022).
[45] M. Hausmann, A. Aaron, A. Amthor, M. Avilov, L. Bandura, R. Bennett, G. Bollen, T. Borden, T. Burgess, S. Chouhan, V. Graves, W. Mittig, D. Morrissey, F. Pellemoine, M. Portillo, R. Ronningen, M. Schein, B. Sherrill, and A. Zeller, Nucl. Instrum. Methods Phys. Res., Sect. B **317**, 349 (2013), xVIth International Conference on ElectroMagnetic Isotope Separators and Techniques Related to their Applications, December 27, 2012 at Matsue, Japan.
[46] T. J. Gray *et al.*, Phys. Rev. Lett. **130**, 242501 (2023).
[47] J. A. Winger, 10.2172/1248341 (2016).

[48] S. Paulauskas, M. Madurga, R. Grzywacz, D. Miller, S. Padgett, and H. Tan, Nucl. Instrum. Methods Phys. Res., Sect. A **737**, 22 (2014).
[49] W. Peters *et al.*, Nucl. Instrum. Methods Phys. Res., Sect. A **836**, 122 (2016).
[50] S. Agostinelli *et al.*, Nucl. Instrum. Methods Phys. Res., Sect. A **506**, 250 (2003).
[51] F. Perrot *et al.*, Phys. Rev. C **74**, 014313 (2006).
[52] Z. Y. Xu *et al.*, Phys. Rev. C **108**, 014314 (2023).
[53] M. Karny, A. Fijałkowska, R. Grzywacz, B. Rasco, K. Rykaczewski, and M. Stepaniuk, Nucl. Instrum. Methods Phys. Res., Sect. B **463**, 390 (2020).
[54] R. Yokoyama *et al.*, Nucl. Instrum. Methods Phys. Res., Sect. B **937**, 93 (2019).
[55] Semiconductor Components Industries, LLC, Silicon photomultipliers (sipm) | array j, https://www.onsemi.com/products/sensors/photodetectors-sipm-spad/silicon-photomultipliers-sipm/arrayj (2023) (accessed: 2023-04-11).
[56] XIA, Pixie-16, https://xia.com/products/pixie-16/ (accessed 9-21-23).
[57] A. Huck, G. Klotz, A. Knipper, C. Miehé, G. Walter, and C. Richard-Serre, Phys. Rev. C **21**, 712 (1980).
[58] A. Huck, G. Klotz, A. Knipper, C. Miehé, G. Walter, and C. Richard-Serre, Phys. Rev. C **18**, 1803 (1978).
[59] M. Wang, W. Huang, F. Kondev, G. Audi, and S. Naimi, Chin. Phys. C **45**, 030003 (2021).
[60] P. Shuai *et al.*, Phys. Rev. C **105**, 054312 (2022).
[61] Z. Y. Xu [Phys. Rev. Lett.] (to be published).
[62] M. Madurga *et al.*, Phys. Rev. Lett. **117**, 092502 (2016).
[63] C. Duke, P. Hansen, O. Nielsen, and G. Rudstam, Nucl. Phys. **A151**, 609 (1970).
[64] J. Orear, *Nuclear Physics, a Course Given by Enrico Fermi at the University of Chicago. Revised Edition* (University of Chicago Press, Chicago, 1950).
[65] J. Papuga, M. L. Bissell, K. Kreim, K. Blaum, B. A. Brown, M. De Rydt, R. F. Garcia Ruiz, H. Heylen, M. Kowalska, R. Neugart, G. Neyens, W. Nörtershäuser, T. Otsuka, M. M. Rajabali, R. Sánchez, Y. Utsuno, and D. T. Yordanov, Phys. Rev. Lett. **110**, 172503 (2013).
[66] F. Touchard, P. Guimbal, S. Büttgenbach, R. Klapisch, M. De Saint Simon, J. Serre, C. Thibault, H. Duong, P. Juncar, S. Liberman, J. Pinard, and J. Vialle, Phys. Lett. **108B**, 169 (1982).
[67] J. K. Smith *et al.*, Phys. Rev. C **102**, 054314 (2020).
[68] N. Shimizu, arXiv:1310.5431.